Originally published 8 February 2018; corrected 29 March 2018

www.sciencemag.org/cgi/content/full/science.aao0702/DC1

Supplementary Materials for

Hippocampal ripples down-regulate synapses

Hiroaki Norimoto, Kenichi Makino,* Mengxuan Gao,* Yu Shikano, Kazuki Okamoto, Tomoe Ishikawa, Takuya Sasaki, Hiroyuki Hioki, Shigeyoshi Fujisawa,† Yuji Ikegaya†

*These authors contributed equally to this work.
†Corresponding author. Email: yuji@ikegaya.jp (Y.I.); fujisawa@brain.riken.jp (S.F.)

Published 8 February 2018 on *Science* First Release
DOI: 10.1126/science.aao0702

This PDF file includes:

Correction: A citation (reference 30 by M. R. Mehta) was mistakenly omitted from the previous version. This error has been corrected.

Materials and Methods:

Animals

The animal experiments were performed with the approval of the animal experiment ethics committee at the University of Tokyo (approval number: 24-10) and RIKEN (approval number: 2015-049, H28-2-215) according to the University of Tokyo and RIKEN guidelines for the care and use of laboratory animals and in accordance with the Fundamental Guidelines for Proper Conduct of Animal Experiment and Related Activities in Academic Research Institutions (Ministry of Education, Culture, Sports, Science and Technology, Notice No. 71 of 2006), the Standards for Breeding and Housing of and Pain Alleviation for Experimental Animals (Ministry of the Environment, Notice No. 88 of 2006), and the Guidelines on the Method of Animal Disposal (Prime Minister's Office, Notice No. 40 of 1995). The mice were housed 2–4 per cage and kept at 22 ± 1°C with *ad libitum* access to food and water on a 12-h light/dark cycle (lights on from 7 a.m. to 7 p.m. (the University of Tokyo) and from 8 a.m. to 8 p.m. (RIKEN)). Adult male C57BL/6J mice, weighing 24–34 g and aged 8–13 weeks, were used for the behavioral experiments. Male C57BL/6J mice and somatostatin (SOM)::channelrhodopsin-2 (ChR2) mice, aged 8-14 weeks, were used for the *in vivo* electrophysiology experiments. Juvenile male or female C57BL/6J mice, SOM-ChR2, Thy1-mGFP mice (*31*), and Arc-dVenus mice (*22*), aged 3 weeks, were used for *in vitro* electrophysiology. Juvenile male or female Arc-dVenus transgenic mice, aged 3 weeks, were used for functional calcium imaging of behaviorally activated neurons.

Drugs

MK801 was applied intraperitoneally at a dose of 0.2 mg/kg. D-2-Amino-5-phosphonopentanoic acid (D-AP5) was dissolved at 10 mM in water and stored at 4°C. Immediately before use, D-AP5 was diluted to its final concentrations with artificial cerebrospinal fluid (aCSF) containing (in mM) 127 NaCl, 3.5 KCl, 1.24 KH_2PO_4, 1.2 $MgSO_4$, 2.0 $CaCl_2$, 26 $NaHCO_3$, and 10 D-glucose.

Object-place recognition task

Before the behavioral task, a 6-day successive handling procedure and 2-day successive 10-min habituation were performed in the behavioral arena, which was a 30×30×30-cm^3 open cubic arena with transparent walls and a smooth brown floor. Objects were used as visual cues. During the encoding periods, two identical objects were placed in the corner of the arena with the visual cue. During the recall periods, one of the objects was displaced to the corner diagonal from the other object. The mice were allowed to explore the arena for 10 min during the encoding periods and for 3 min during the recall periods. The encoding and recall periods were separated by a home-cage resting period of 2 h and began at 7:30-8:30 and 9:30-10:30 PM, respectively. A discrimination ratio was calculated for each mouse as T2/(T1+T2), where T1 and T2 represent the time spent exploring the familiar object and the displaced object, respectively. The arena and objects were cleaned with 70% ethanol before each experiment. Exploration was defined as sniffing or touching the object with the nose or forepaws. Sitting on the object was not considered exploration. All trials were recorded using a top-view camera, and the exploration time was measured by an experimenter blinded to the behavioral conditions.

All animals were allowed to explore the novel environment for 30 min before the closed-loop stimulation session began.

Animal preparations and *in vivo* electrophysiology

Three C57BL/6J mice and twelve SOM::ChR2-EYFP mice were implanted with silicon probes for chronic recordings of neuronal activity. The general surgical procedures for chronic recordings were described in our previous paper (*32*). We used Buzsaki32 or A4×8 multichannel probes that consisted of 4 shanks (200 µm/400 µm shank separation); each shank had 8 recording sites that were staggered to provide a two-dimensional arrangement at a vertical separation of 20 µm/100 µm. The mice were implanted with a silicon probe in the CA1 area (AP = -1.9 mm, ML = 1.7 mm; the shanks were aligned parallel to the septotemporal axis of the hippocampus, *i.e.*, 45º parasagittal). The silicon probe was attached to a micromanipulator and was moved gradually to the desired depth position. After the initial surgery, every animal was singly housed. During the recording sessions, the wide-band neurophysiological signals were acquired continuously at 20 kHz. The wide-band signal was down-sampled to 1.25 kHz and was used as the local field potential (LFP) signal. Spike sorting was performed (*33*), followed by manual adjustment of the clusters. Each unit was classified as a putative pyramidal cell or an interneuron based on the spike waveform, firing rate, and autocorrelograms (*15*). The mice were equipped with an LED to track their head movements. Recordings were carried out in a home cage (W150×D150×H150 mm^3) or a novelty box (a box of a different form of the home cage with novel objects). Slow-wave (SW) states were detected using the ratio of the power in the theta band (6–10 Hz) to the delta band (1–4 Hz) of the LFPs, followed by manual adjustment with the aid of visual inspection, time-resolved power spectra, and head movement data (Fig. S1). The manual adjustment was conducted to remove falsely detected short segments of data and epochs containing movement artifacts. To investigate the breakdown of SW states, another set of animals was used. Five C57BL/6J mice were implanted with tetrodes into the hippocampus and the prefrontal cortex for chronic LFP recordings and with stainless-steel wires into the neck muscles for electromyogram (EMG) recordings. Each LFP electrode consisted of 6 independent tetrodes and was made of a 17-µm-wide polyimide-coated platinum-iridium (90/10%) wire, the tip of which was plated with platinum to lower electrode impedances to 150–300 kΩ. The electrodes were stereotaxically implanted above the hippocampus (1.9 mm posterior and 1.7 mm lateral to bregma) and the frontal cortex (1.65 mm anterior and 0.3 mm lateral to bregma). An incision was made at the incised neck area, and the EMG electrode wire was sutured to the dorsal neck muscles. A ground/reference electrode was placed on the cerebellum, and a recording device was secured to the skull using stainless steel screws and dental cement. Then, the LFP electrodes were advanced to the targeted brain regions for at least one week after the surgery. Recordings were sampled at 2 kHz and filtered between 0.1 and 500 Hz. To monitor the rat's moment-to-moment position, their infrared signal was tracked at 15 Hz using a video camera attached to the ceiling. Awake immobility periods were detected semi-automatically based on EMG. For field excitatory postsynaptic potential (fEPSP) recordings, tungsten bipolar electrodes were implanted to stimulate the CA1 stratum radiatum. A 100-µs duration pulse was given every 20 s. The stimulus intensity was set to the intensity that resulted in an fEPSP with a slope 30–50% of the maximum, ranging between 60–90 µA.

For place cell identification, the recording arena was divided into bins of approximately 2×2 cm^2 to generate spike count maps for each unit and an occupancy map (time spent by the animal in each bin). All maps were then smoothed by convolution with a Gaussian kernel with a standard deviation equal to one bin width. Finally, spatial rate maps were generated by normalizing the smoothed spike count maps by the smoothed occupancy map. Cells that showed remapping between the sessions were excluded from the analysis (*34*).

Real-time feedback delivery of light stimulation with the optogenetic technique

We used transgenic mice that expressed ChR2 (*35*) under the SOM promoter. We chose these mice because oriens–lacunosum moleculare (O-LM) interneurons in the CA3 region are more silent during sharp waves/ripples (SWRs) than other subtypes of interneurons (*36*) and thus are expected to efficiently suppress SWRs upon artificial activation (*15*). One or more optical fibers coupled with blue laser diodes (450 nm) were attached to a microdrive parallel to the silicon probes (Buzsaki32 or A4×8) (*37*) so that the tip of the optic fiber could be placed in the CA3 pyramidal cell layer and the silicon probes in the CA1 pyramidal cell layer. The light power was set to 5–20 mW at the end of the fiber. A single channel from the middle of the CA1 pyramidal cell layer was selected for real-time processing by a programmable digital signal processor running at 25 kHz. The root mean square (RMS) of the bandpass filtered (140–250 Hz) signal was computed in two running windows, long (2 s; RMS1) and short (8 ms; RMS2). Ripples were defined as events with an RMS2 exceeding 4×RMS1 for at least 8 ms, enabling the reliable online detection of the majority of ripples during their two or three cycles (confirmed by *post hoc* offline detection). Light stimulation was applied either under light (detection and stimulation) conditions or delayed (detection and 80-to-120-ms-delayed stimulation) conditions. The optogenetic stimulation was delivered 23 ± 12 ms after the onset of the SWR. When the false stimulation rate was estimated using local field potential (LFP) traces of the Sham sessions in which no light stimulation was immediately applied upon SWR detection, the false positive illumination rate 19.2 ± 1.0%, whereas the false negative rate was 2.3 ± 1.8%. The false-positive events were typically due to muscle movement artifacts. For the *in vitro* experiments, we used a custom-built routine running a script that read the signal from an amplifier. When the amplitude of the LFP crossed a manually set value, a light illumination was triggered through a digital signal with a modifiable delay and duration. Light was applied at powers of 0.05-0.2 mW.

Slice preparations

Wild-type, SOM::ChR2-EYFP, Thy1-mGFP, or Arc-dVenus transgenic C57BL/6J mice of either sex (3 weeks old) were placed in a novel chamber (280 mm wide, 300 mm long, 250 mm high) and were allowed to explore for 30 min. The mice were deeply anesthetized with diethyl ether and decapitated. The brains were removed quickly, and oblique or horizontal hippocampal slices (400 μm thick) were prepared using a vibratome in ice-cold, oxygenated cutting solution consisting of (in mM) 222.1 sucrose, 27 $NaHCO_3$, 1.4 NaH_2PO_4, 2.5 KCl, 1 $CaCl_2$, 7 $MgSO_4$, and 0.5 ascorbic acid (*16*). The slices were allowed to recover for at least 60 min and then submerged in a chamber filled

with oxygenated aCSF at 35–37°C. The aCSF consisted of (in mM) 127 NaCl, 1.6 KCl, 1.24 KH_2PO_4, 1.3 $MgSO_4$, 2.0 $CaCl_2$, 26 $NaHCO_3$, and 10 D-glucose for recordings (*38*).

In vitro electrophysiology

The slices were transferred to a recording chamber continuously perfused with aCSF at 32–33°C. The stimuli were delivered through a tungsten electrode, and fEPSPs were recorded using glass pipettes filled with aCSF or an 8×8 planar multi-electrode array (electrode size: 50×50 mm; inter-polar interval: 150 mm). The electrodes were carefully placed in the CA1 stratum radiatum within a distance of 100 μm from the pyramidal cell layer. A 100-μs pulse was given every 30 s. The stimulus intensity was set to result in an fEPSP with a slope of approximately 30% of the maximum fEPSP slope, ranging between 30–70 μA. Electrophysiological data were acquired using pCLAMP 10. The signals were low-pass filtered at 2 kHz and digitized at 20 kHz. The changes in fEPSP slope were expressed as percent changes in the initial slope relative to the mean slope during the baseline period. SWRs and multiunits were recorded using borosilicate glass pipettes (1–2 MΩ) filled with aCSF. The traces were bandpass filtered between 2 and 30 Hz for the LFP and were high-pass filtered at 300 Hz for multiunit recordings. Then, SWRs were detected at a threshold of 5× s.d. of the baseline noise. The detected events were visually scrutinized and manually rejected if they were erroneously detected. SWRs with event durations of less than 30 ms were also discarded because these events were typically artifacts. Because SWRs lasted for approximately 100 ms, we defined the activity that occurred within 100 ms before and after the SWR peak time as SWR-relevant activity by considering video frame jitters. In the experiments depicted in Fig. S6 and S8, to ensure that the tissue had recovered from slicing, we waited until the slice preparations began to emit SWRs at an event frequency of at least 0.8 Hz before beginning recordings. Then, the SWR event frequency gradually increased and peaked before the spontaneous decrease observed in SWR-emitting slices. Thus, for each slice, the time of the maximal SWR event frequency was defined as time 0 min, to which individual data were aligned for normalization.

Immunohistochemistry

The mice were anesthetized with isoflurane and perfused transcardially with cold phosphate-buffered saline (PBS; 1.47×10^{-3} M KH_2PO_4, 8.10×10^{-3} M $Na_2HPO_4\cdot12H_2O$, 2.68×10^{-3} M KCl, 1.37×10^{-1} M NaCl) followed by 4% paraformaldehyde. The brain samples were post-fixed with 4% paraformaldehyde for 4 h at 4°C and subsequently immersed in 15% and 30% sucrose for 24 h at 4°C. The brain area including the hippocampus was coronally sectioned at a thickness of 40 μm using a cryostat at -24°C. The sections were permeabilized for 30 min at room temperature in PBS with 0.3% Triton X-100 and 10% goat serum and incubated with the anti-GFP primary antibody (Chicken, 1:1000; #ab13970, Abcam, Cambridge, UK) in PBS with 0.3% Triton X-100 and 10% goat serum overnight at room temperature. After rinsing with PBS, the samples were incubated with a secondary antibody conjugated with Alexa Fluor dyes (Goat, 1:500; Invitrogen, Gaithersburg, MD, USA) and NeuroTrace 435/455 blue-fluorescent Nissl stain (1:500; #N21479, Thermo Fisher Scientific, Rockford, IL, USA) in PBS with 10% goat serum for 4 h at room temperature. After the samples were rinsed with PBS,

they were mounted with Permafluor (#TA-030-FM, Thermo Fisher Scientific, Rockford, IL, USA). Images were acquired using a FV1200 confocal system under a 20× objective.

Calcium imaging

Functional multineuron calcium imaging was conducted locally by loading cells with Fura-2AM, which can detect single spikes. Fura-2AM was dissolved in DMSO containing 10% Pluronic F-127 to yield a concentration of 200 μM. Immediately before use, this solution was diluted ten-fold with aCSF and loaded into pipettes (3–5 MΩ). The tip of the pipette was inserted into an acute horizontal slice, and a pressure of 50–60 hPa was applied for 3–5 min using a 10-ml syringe pressurizer. Fluorophores were excited at 405 nm with a laser diode and visualized using 507-nm-long pass emission filters. Videos were recorded for 3 min at 50 frames/s using a 16× objective (0.8 numerical aperture), a spinning-disk confocal microscope, and a cooled CCD camera or a CMOS embedded in an upright microscope. The fluorescence change was measured as $(F_t - F_0)/F_0$, where F_t is the fluorescence intensity at time t, and F_0 is the background fluorescence intensity between -10 to 10 s relative to t. Using a principal component analysis and a support vector machine optimized to calcium imaging, spike-elicited calcium transients were semiautomatically detected with a custom-written program in Visual Basic (*38*). Baseline noise was removed using the Okada filter (*39*). To examine the effect of D-AP5 perfusion on spontaneous neuronal activity, baseline activity was recorded for 3 min, and then 50 μM D-AP5 was bath-applied. Activity during the D-AP5 perfusion was recorded from 40 min to 43 min after the initiation of the perfusion. dVenus was excited at 488 nm and visualized using a 520/535-nm bandpass emission filter after 2 h of recording sessions. The response probability of individual dVenus(+) and dVenus(-) neurons was compared between 0–3 min and 40–43 min. The mean probability that a given cell exhibited a calcium transient during a single SWR event was defined as the SW participation probability of the cell.

Two-photon imaging

The dendrites of CA1 pyramidal cells in slices prepared from Thy1-GFP mice were imaged using a two-photon laser-scanning microscope. Fluorophores were excited at 900 nm, and fluorescence images were collected through a water-immersion 25× objective lens (1.05 NA). The first set of images was taken 5 min after the SWR event frequency reached 0.80 Hz. Regions of dendrites (usually second or third order branches) that had 5–34 spines were selected and time-lapse imaged at a higher magnification (optical zoom = 5×). Images were taken every 15 min at a resolution of 512×512 or 256×256 pixels. The spine head volume was estimated as $4\pi(\varphi/2)^3/3$, in which φ represents the head width of the spine (*40*). The head width was measured from the maximum spine area across a series of *Z*-step images (0.5 μm steps). The distance from the center of gravity of the spine head to the stem dendrite was measured as the spine neck length. Spines were classified into stubby, thin, or mushroom based on their length, spine head diameter, and neck diameter using IMARIS software (*41, 42*). The data were analyzed by experimenters who were unaware of the experimental conditions

Data analysis

Values are reported as the mean with individual data points or mean ± s.e.m., except for the data in Fig. S8B and S8C, which used geometric mean ± s.e.m. and whisker plots composed of the median (central line in the box), ranges between the 25th and 75th percentile (box) and between the 10th and 90th percentiles (whiskers). Data analyses were performed in a blind fashion.

Primary numerical data sets is available online (URL: http://ikegaya.jp/data/norimoto_science2018/)

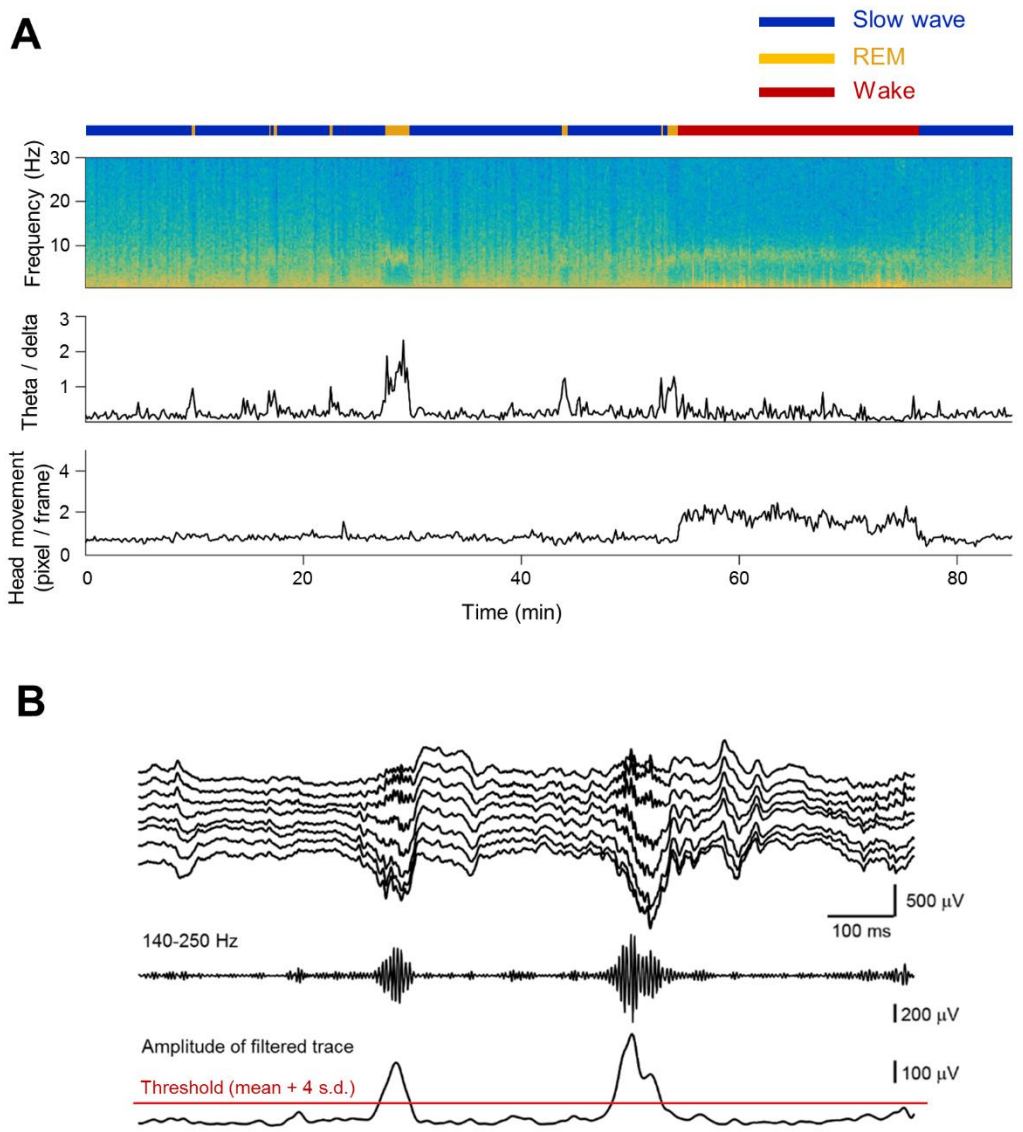

Fig. S1. Classification of brain states. (**A**) Time-resolved power spectrum of an LFP trace recorded from the hippocampal CA1 region. The two bottom plots indicate the theta/delta ratio and head movements, which were used to define brain states, *i.e.*, slow-wave state, rapid eye movement (REM) state, and waking state. (**B**) The threshold for SWR detection was set to 4× s.d. above the mean power. Top, raw LFP traces recorded from the CA1 region; Middle, a trace filtered in a ripple-frequency (140–250 Hz) band; Bottom, a trace representing the LFP envelope amplitude (power).

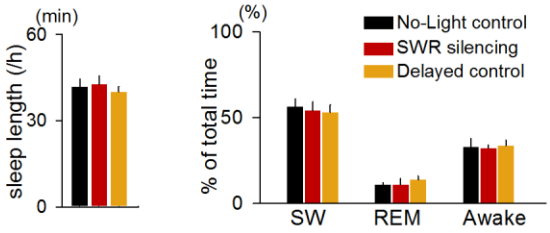

Fig. S2. SWR silencing does not affect sleep quality. Left: the total sleep length during the 7-h SWR silencing period did not differ among the groups. $P = 0.79$, $F_{2,13} = 0.236$, one-way ANOVA. Right: the percentages of SW, REM, and awake states did not differ during SWR silencing. SW: $P = 0.89$, $F_{2,15} = 0.12$, REM: $P = 0.68$, $F_{2,15} = 0.40$, Awake: $P = 0.97$, $F_{2,15} = 0.035$, one-way ANOVA.

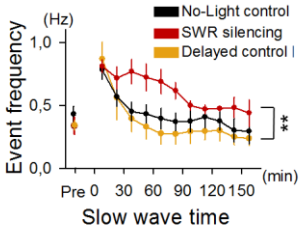

Fig. S3. The SWR-silenced group shows higher SWR event frequencies than the delayed control group throughout the recording time. Silencing *vs.* no-light control: ** $P = 1.2\times10^{-5}$, $F_{1,106} = 21.2$, Silencing vs. delayed control: **$P = 6.5\times10^{-8}$, $F_{1,81} = 36.8$, two-way ANOVA. n = 6-7 mice.

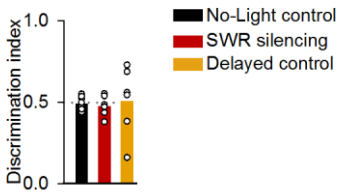

Fig. S4. No behavioral differences were observed in the encoding phase of the object-place recognition task. The percentage of time spent exploring two identical objects did not differ between the SWR silencing, the delayed control, and the no-light control (P = 0.54, H_2 = 1.23, Kruskal-Wallis one -way ANOVA on ranks, n = 6-7 mice).

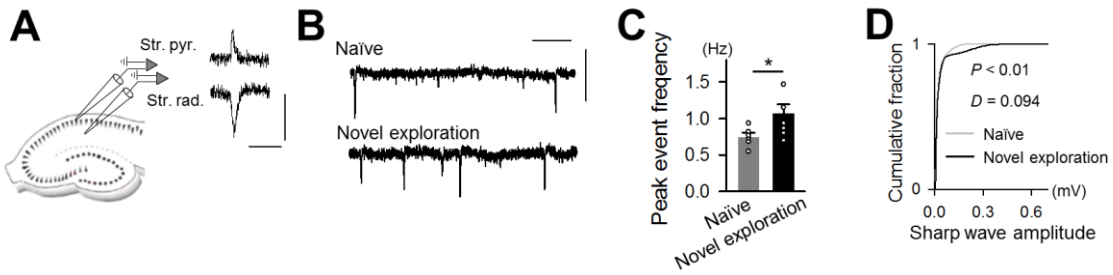

Fig. S5. Spatial exploration increases the event frequency of SWRs in hippocampal slice preparation. (**A**) SWRs were recorded from the CA1 stratum radiatum and the pyramidale. Scale bars = 100 ms and 0.1 mV. (**B**) Representative raw LFP traces recorded from the stratum radiatum of the hippocampal slices prepared from naïve mice (top) and mice that had explored a novel environment for 30 min (bottom). Scale bars = 1 s and 0.1 mV. (**C**) Slices prepared from mice that had experienced spatial exploration exhibited higher SWR event frequencies than slices from naïve mice. **P* = 0.043, t_{10} = -1.90, one-tailed *t*-test. *n* = 6 slices from 6 mice. (D) Slices prepared from mice that had experienced spatial exploration exhibited higher SWR amplitudes than slices from naïve mice. *P* = 4.6×10^{-32}, D_{22195} = 0.094, Kolmogorov-Smirnov test. *n* = 5467 and 16731 events.

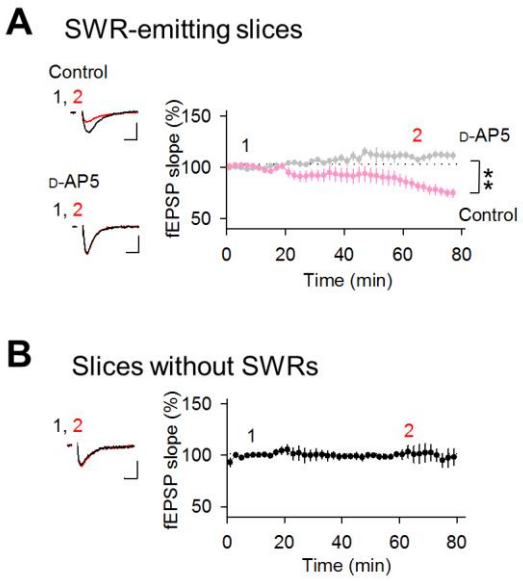

Fig. S6. Spontaneous depression of fEPSPs in SWR-emitting slices. (**A**) SWRs and fEPSPs were recorded in the continuous presence or absence of 50 µM D-AP5 from the CA1 stratum radiatum of hippocampal slices prepared from mice that had explored a novel environment for 30 min. A stimulating electrode was placed on the CA1 stratum radiatum. The fEPSP slopes were normalized to the 20-min baseline values. The insets show typical fEPSP traces at the times indicated by 1 and 2. Scale bars = 10 ms and 50 µV. The fEPSP slopes gradually declined over time but did not decline in the presence of D-AP5. $^{**}P = 3.0\times10^{-41}$, $F_{1,240} = 270.8$, two-way ANOVA, $n = 5$ each. (**B**) LTD was not induced in conventional slices that did not emit SWRs. $n = 4$ slices. Scale bars = 10 ms and 50 µV.

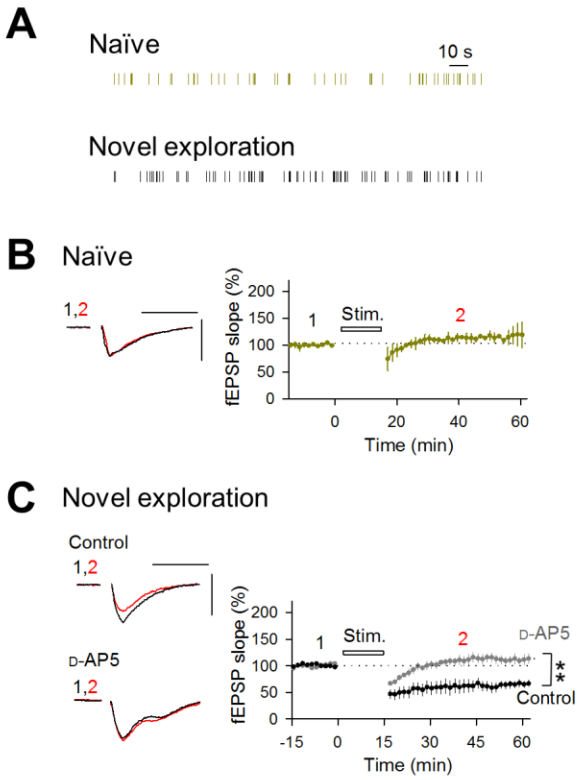

Fig. S7. Repetitive stimulation patterned from *in vivo* SWR timings leads to long-term depression. (**A**) Examples of stimulation patterns that were applied to the Schaffer collaterals (parts). These SWR timings were obtained for 15 min during *in vivo* SW states of naïve mice and mice that had explored a novel environment for 30 min. (**B**) Stimulation patterned from SWR timings in naïve mice did not induce LTD in conventional slices that did not emit SWRs (n = 3 slices). (**C**) Stimulation patterned from SWR timings after spatial explorations induced LTD, which was blocked by a bath application of 50 µM D-AP5. $^{**}P = 2.5\times10^{-46}$, $F_{1,376} = 271.7$, two-way ANOVA, n = 5 slices each. The insets in each panel show typical fEPSP traces at times 1 and 2. Scale bars = 20 ms and 1 mV.

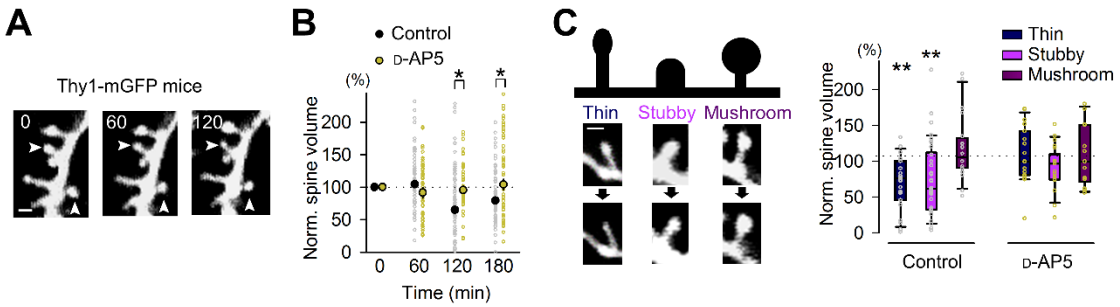

Fig. S8. SWR-emitting slices exhibit NMDAR-dependent spontaneous spine shrinkage. (A) Time-lapse two-photon imaging of dendritic spines on an apical dendrite of a CA1 pyramidal neuron in a slice prepared from a Thy1-GFP mouse. Arrowheads indicate spines that shrank. (B) Percentage changes in the volume of the spine heads during SWRs in the presence or absence of 50 µM D-AP5. Time 0 is aligned at the time of the maximal frequencies of SWR events. 120 min: $*P = 0.014$, $Z = 2.47$, 180 min: $*P < 1.0\times10^{-30}$, $Z = 8.24$, Wilcoxon signed rank test, Control: $n = 77$ spines from 4 slices from 4 mice; D-AP5: $n = 55$ spines of 5 slices from 5 mice. (C) Thin and stubby types but not mushroom types spontaneously shrank at 120 min. D-AP5 prevented spine shrinkage. Scale bar = 1 µm. Thin: $**P = 2.0\times10^{-5}$, $Z = 4.11$; Stubby: $**P = 5.9\times10^{-7}$, $Z = 4.86$, one-sample signed rank test, Control: $n = 20$–31 spines, D-AP5: $n = 14$–21 spines

References and Notes

1. V. V. Vyazovskiy, C. Cirelli, M. Pfister-Genskow, U. Faraguna, G. Tononi, Molecular and electrophysiological evidence for net synaptic potentiation in wake and depression in sleep. *Nat. Neurosci.* **11**, 200–208 (2008). doi:10.1038/nn2035 Medline

2. R. Huber, H. Mäki, M. Rosanova, S. Casarotto, P. Canali, A. G. Casali, G. Tononi, M. Massimini, Human cortical excitability increases with time awake. *Cereb. Cortex* **23**, 332–338 (2013). doi:10.1093/cercor/bhs014 Medline

3. G. Tononi, C. Cirelli, Sleep and synaptic homeostasis: A hypothesis. *Brain Res. Bull.* **62**, 143–150 (2003). doi:10.1016/j.brainresbull.2003.09.004 Medline

4. G. Tononi, C. Cirelli, Sleep and the price of plasticity: From synaptic and cellular homeostasis to memory consolidation and integration. *Neuron* **81**, 12–34 (2014). doi:10.1016/j.neuron.2013.12.025 Medline

5. A. K. Lee, M. A. Wilson, Memory of sequential experience in the hippocampus during slow wave sleep. *Neuron* **36**, 1183–1194 (2002). doi:10.1016/S0896-6273(02)01096-6 Medline

6. V. Ego-Stengel, M. A. Wilson, Disruption of ripple-associated hippocampal activity during rest impairs spatial learning in the rat. *Hippocampus* **20**, 1–10 (2010). Medline

7. G. Girardeau, K. Benchenane, S. I. Wiener, G. Buzsáki, M. B. Zugaro, Selective suppression of hippocampal ripples impairs spatial memory. *Nat. Neurosci.* **12**, 1222–1223 (2009). doi:10.1038/nn.2384 Medline

8. G. M. van de Ven, S. Trouche, C. G. McNamara, K. Allen, D. Dupret, Hippocampal offline reactivation consolidates recently formed cell assembly patterns during sharp wave-ripples. *Neuron* **92**, 968–974 (2016). doi:10.1016/j.neuron.2016.10.020 Medline

9. J. H. Sadowski, M. W. Jones, J. R. Mellor, Sharp-wave ripples orchestrate the induction of synaptic plasticity during reactivation of place cell firing patterns in the hippocampus. *Cell Rep.* **14**, 1916–1929 (2016). doi:10.1016/j.celrep.2016.01.061 Medline

10. E. V. Lubenov, A. G. Siapas, Decoupling through synchrony in neuronal circuits with propagation delays. *Neuron* **58**, 118–131 (2008). doi:10.1016/j.neuron.2008.01.036 Medline

11. L. L. Colgin, D. Kubota, Y. Jia, C. S. Rex, G. Lynch, Long-term potentiation is impaired in rat hippocampal slices that produce spontaneous sharp waves. *J. Physiol.* **558**, 953–961 (2004). doi:10.1113/jphysiol.2004.068080 Medline

12. O. Bukalo, E. Campanac, D. A. Hoffman, R. D. Fields, Synaptic plasticity by antidromic firing during hippocampal network oscillations. *Proc. Natl. Acad. Sci. U.S.A.* **110**, 5175–5180 (2013). doi:10.1073/pnas.1210735110 Medline

13. O. Eschenko, W. Ramadan, M. Mölle, J. Born, S. J. Sara, Sustained increase in hippocampal sharp-wave ripple activity during slow-wave sleep after learning. *Learn. Mem.* **15**, 222–228 (2008). doi:10.1101/lm.726008 Medline

14. C. J. Behrens, L. P. van den Boom, L. de Hoz, A. Friedman, U. Heinemann, Induction of sharp wave-ripple complexes in vitro and reorganization of hippocampal networks. *Nat. Neurosci.* **8**, 1560–1567 (2005). doi:10.1038/nn1571 Medline

15. E. Stark, L. Roux, R. Eichler, Y. Senzai, S. Royer, G. Buzsáki, Pyramidal cell-interneuron interactions underlie hippocampal ripple oscillations. *Neuron* **83**, 467–480 (2014). doi:10.1016/j.neuron.2014.06.023 Medline

16. M. Mizunuma, H. Norimoto, K. Tao, T. Egawa, K. Hanaoka, T. Sakaguchi, H. Hioki, T. Kaneko, S. Yamaguchi, T. Nagano, N. Matsuki, Y. Ikegaya, Unbalanced excitability underlies offline reactivation of behaviorally activated neurons. *Nat. Neurosci.* **17**, 503–505 (2014). doi:10.1038/nn.3674 Medline

17. G. L. Collingridge, S. J. Kehl, H. McLennan, Excitatory amino acids in synaptic transmission in the Schaffer collateral-commissural pathway of the rat hippocampus. *J. Physiol.* **334**, 33–46 (1983). doi:10.1113/jphysiol.1983.sp014478 Medline

18. M. Matsuzaki, G. C. Ellis-Davies, T. Nemoto, Y. Miyashita, M. Iino, H. Kasai, Dendritic spine geometry is critical for AMPA receptor expression in hippocampal CA1 pyramidal neurons. *Nat. Neurosci.* **4**, 1086–1092 (2001). doi:10.1038/nn736 Medline

19. M. Masugi-Tokita, E. Tarusawa, M. Watanabe, E. Molnár, K. Fujimoto, R. Shigemoto, Number and density of AMPA receptors in individual synapses in the rat cerebellum as revealed by SDS-digested freeze-fracture replica labeling. *J. Neurosci.* **27**, 2135–2144 (2007). doi:10.1523/JNEUROSCI.2861-06.2007 Medline

20. Q. Zhou, K. J. Homma, M. M. Poo, Shrinkage of dendritic spines associated with long-term depression of hippocampal synapses. *Neuron* **44**, 749–757 (2004). doi:10.1016/j.neuron.2004.11.011 Medline

21. O. Paulsen, T. J. Sejnowski, Natural patterns of activity and long-term synaptic plasticity. *Curr. Opin. Neurobiol.* **10**, 172–179 (2000). doi:10.1016/S0959-4388(00)00076-3 Medline

22. M. Eguchi, S. Yamaguchi, In vivo and in vitro visualization of gene expression dynamics over extensive areas of the brain. *Neuroimage* **44**, 1274–1283 (2009). doi:10.1016/j.neuroimage.2008.10.046 Medline

23. D. Balduzzi, G. Tononi, What can neurons do for their brain? Communicate selectivity with bursts. *Theory Biosci.* **132**, 27–39 (2013). doi:10.1007/s12064-012-0165-0 Medline

24. S. S. Yoo, P. T. Hu, N. Gujar, F. A. Jolesz, M. P. Walker, A deficit in the ability to form new human memories without sleep. *Nat. Neurosci.* **10**, 385–392 (2007). doi:10.1038/nn1851 Medline

25. G. S. Lynch, T. Dunwiddie, V. Gribkoff, Heterosynaptic depression: A postsynaptic correlate of long-term potentiation. *Nature* **266**, 737–739 (1977). doi:10.1038/266737a0 Medline

26. R. M. Mulkey, R. C. Malenka, Mechanisms underlying induction of homosynaptic long-term depression in area CA1 of the hippocampus. *Neuron* **9**, 967–975 (1992). doi:10.1016/0896-6273(92)90248-C Medline

27. S. M. Dudek, M. F. Bear, Homosynaptic long-term depression in area CA1 of hippocampus and effects of N-methyl-D-aspartate receptor blockade. *Proc. Natl. Acad. Sci. U.S.A.* **89**, 4363–4367 (1992). doi:10.1073/pnas.89.10.4363 Medline

28. L. de Vivo, M. Bellesi, W. Marshall, E. A. Bushong, M. H. Ellisman, G. Tononi, C. Cirelli, Ultrastructural evidence for synaptic scaling across the wake/sleep cycle. *Science* **355**, 507–510 (2017). doi:10.1126/science.aah5982 Medline

29. G. H. Diering, R. S. Nirujogi, R. H. Roth, P. F. Worley, A. Pandey, R. L. Huganir, Homer1a drives homeostatic scaling-down of excitatory synapses during sleep. *Science* **355**, 511–515 (2017). doi:10.1126/science.aai8355 Medline

30. M. R. Mehta, Cortico-hippocampal interaction during up-down states and memory consolidation. *Nat. Neurosci.* **10**, 13-15 (2007). doi:10.1038/nn0107-13 Medline

31. G. Feng, R. H. Mellor, M. Bernstein, C. Keller-Peck, Q. T. Nguyen, M. Wallace, J. M. Nerbonne, J. W. Lichtman, J. R. Sanes, Imaging neuronal subsets in transgenic mice expressing multiple spectral variants of GFP. *Neuron* **28**, 41–51 (2000). doi:10.1016/S0896-6273(00)00084-2 Medline

32. S. Fujisawa, A. Amarasingham, M. T. Harrison, G. Buzsáki, Behavior-dependent short-term assembly dynamics in the medial prefrontal cortex. *Nat. Neurosci.* **11**, 823–833 (2008). doi:10.1038/nn.2134 Medline

33. S. N. Kadir, D. F. Goodman, K. D. Harris, High-dimensional cluster analysis with the masked EM algorithm. *Neural Comput.* **26**, 2379–2394 (2014). doi:10.1162/NECO_a_00661 Medline

34. S. Leutgeb, J. K. Leutgeb, A. Treves, M. B. Moser, E. I. Moser, Distinct ensemble codes in hippocampal areas CA3 and CA1. *Science* **305**, 1295–1298 (2004). doi:10.1126/science.1100265 Medline

35. E. S. Boyden, F. Zhang, E. Bamberg, G. Nagel, K. Deisseroth, Millisecond-timescale, genetically targeted optical control of neural activity. *Nat. Neurosci.* **8**, 1263–1268 (2005). doi:10.1038/nn1525 Medline

36. T. Klausberger, P. J. Magill, L. F. Márton, J. D. Roberts, P. M. Cobden, G. Buzsáki, P. Somogyi, Brain-state- and cell-type-specific firing of hippocampal interneurons in vivo. *Nature* **421**, 844–848 (2003). doi:10.1038/nature01374 Medline

37. S. Royer, B. V. Zemelman, M. Barbic, A. Losonczy, G. Buzsáki, J. C. Magee, Multi-array silicon probes with integrated optical fibers: Light-assisted perturbation and recording of local neural circuits in the behaving animal. *Eur. J. Neurosci.* **31**, 2279–2291 (2010). doi:10.1111/j.1460-9568.2010.07250.x Medline

38. H. Norimoto, M. Mizunuma, D. Ishikawa, N. Matsuki, Y. Ikegaya, Muscarinic receptor activation disrupts hippocampal sharp wave-ripples. *Brain Res.* **1461**, 1–9 (2012). doi:10.1016/j.brainres.2012.04.037 Medline

39. M. Okada, T. Ishikawa, Y. Ikegaya, A computationally efficient filter for reducing shot noise in low S/N data. *PLOS ONE* **11**, e0157595 (2016). doi:10.1371/journal.pone.0157595 Medline

40. N. Takahashi, K. Kitamura, N. Matsuo, M. Mayford, M. Kano, N. Matsuki, Y. Ikegaya, Locally synchronized synaptic inputs. *Science* **335**, 353–356 (2012). doi:10.1126/science.1210362 Medline

41. A. Peters, I. R. Kaiserman-Abramof, The small pyramidal neuron of the rat cerebral cortex. The perikaryon, dendrites and spines. *Am. J. Anat.* **127**, 321–355 (1970). doi:10.1002/aja.1001270402 Medline

42. K. M. Harris, F. E. Jensen, B. Tsao, Three-dimensional structure of dendritic spines and synapses in rat hippocampus (CA1) at postnatal day 15 and adult ages: Implications for the maturation of synaptic physiology and long-term potentiation. *J. Neurosci.* **12**, 2685–2705 (1992). Medline